

CIRCUMNUCLEAR KEPLERIAN DISKS IN GALAXIES¹

FRANCESCO BERTOLA,² MICHELE CAPPELLARI,² JOSÉ G. FUNES, S.J.,² ENRICO M. CORSINI,²
ALESSANDRO PIZZELLA³, AND JUAN C. VEGA BELTRÁN⁴

Received 1998 June 25; accepted 1998 October 20; published 1998 November 12

ABSTRACT

In this Letter, we demonstrate the possibility of inferring the presence of Keplerian gaseous disks using properly equipped optical ground-based telescopes. We have modeled the peculiar bidimensional shape of the emission lines in a sample of five early-type disk galaxies as due to the motion of a gaseous disk rotating in the combined potential of a central pointlike mass and of an extended stellar disk. The value of the central mass concentration estimated for four galaxies of the sample (NGC 2179, NGC 4343, NGC 4435, and NGC 4459) is $\sim 10^9 M_{\odot}$. This value, according to the assumptions made in our model, is overestimated. However, we have calculated that the effect is well within the errors. For the remaining galaxy, NGC 5064, an upper limit of $5 \times 10^7 M_{\odot}$ is estimated.

Subject headings: black hole physics — galaxies: kinematics and dynamics — galaxies: nuclei — galaxies: structure

1. INTRODUCTION

There is an increasing amount of evidence of conspicuous mass concentrations in the center of galaxies, lending support to the idea that their central engine consists of a black hole (for recent reviews, see Kormendy & Richstone 1995; Ho 1998). This evidence comes both from stellar and gaseous dynamics. In this latter case, the mass concentration is deduced by the observation of an increase toward the center of the rotation velocity of the gaseous disk, according to Kepler's third law. Seven circumnuclear Keplerian disks (CNKDs) have been observed up to now: four have been discovered in elliptical galaxies using the high-resolution capability of the *Hubble Space Telescope (HST)* (Ferrarese, Ford, & Jaffe 1996; Macchetto et al. 1997; Bower et al. 1998; van der Marel & van den Bosch 1998), while three were detected in spirals with VLBI and VLBA observations of maser sources (Miyoshi et al. 1995; Greenhill & Gwinn 1997; Greenhill, Moran, & Herrnstein 1997).

In a program aimed to study with high spatial and spectral resolution the structure of the emission lines in the nuclear regions of early-type disk galaxies, we have obtained, with the 3.6 m telescope at La Silla, major-axis spectra of the Sa galaxies NGC 2179 and NGC 5064. In the first case it is possible to recognize, applying our modeling technique, the kinematical behavior typical of a CNKD, while the second represents a limiting case for its detection with our instrumental setup. In addition, we apply our modeling to three early-type disk galaxies (NGC 4343, NGC 4435, and NGC 4459) observed by Rubin, Kenney, & Young (1997), showing that also in these cases the shape of the emission lines is consistent with the presence of CNKDs. In this way we demonstrate the feasibility

of detecting CNKDs with optical ground-based telescopes. The general data on the galaxies studied are given in Table 1.

2. OBSERVATIONS AND DATA REDUCTION

The spectroscopic observations of NGC 2179 and NGC 5064 were carried out at the 3.6 m ESO Telescope in La Silla on 1997 February 3–4. The telescope was equipped with the Cassegrain Echelle Spectrograph on which was mounted the Long Camera in long-slit configuration without the cross-disperser. The 31.6 lines mm^{-1} grating was used in combination with a $1'3 \times 2'4$ slit. The spectral order number 86 ($\lambda_c = 6617 \text{ \AA}$) corresponding to the redshifted $H\alpha$ region was isolated by means of the narrowband 6630/51 \AA filter. It yielded a wavelength coverage of about 78 \AA between 6593 and 6670 \AA with a reciprocal dispersion of 3.17 \AA mm^{-1} . The adopted detector was the number 37 1024 \times 1024 TK1024AB CCD with a 24 \times 24 μm^2 pixel size. No on-chip binning was applied, and each pixel corresponds to 0.076 \AA .

We took for NGC 2179 and NGC 5064 six and four separate major-axis spectra (P.A. = 170° and P.A. = 38°, respectively) centered on the nucleus for a total exposure time of 360 and 240 minutes, respectively. The galaxies were centered on the slit using the guiding camera at the beginning of each exposure. Comparison thorium-argon lamp exposures were obtained before and after each object integration. The value of the seeing FWHM during the observing nights was between 0'8 and 1'2 as measured by the La Silla Differential Image Motion Monitor. Using standard MIDAS routines, the spectra were bias-subtracted, flat-field corrected, cleaned for cosmic rays, and wavelength calibrated. Cosmic rays were identified by comparing the counts in each pixel with the local mean and standard deviation and then corrected by substituting a suitable value. The instrumental resolution was derived by measuring the FWHM of ~ 30 single emission lines distributed all over the spectral range of a calibrated comparison spectrum. It corresponds to a FWHM of $0.233 \pm 0.017 \text{ \AA}$ (i.e., $\sim 11 \text{ km s}^{-1}$ at $H\alpha$). The single spectra of the same object were aligned and co-added using their stellar-continuum centers as reference. In each spectrum, the center of the galaxy was defined by the center of a Gaussian fit to the radial profile of the stellar continuum. The contribution of the sky was determined from the edges of the resulting frame and then subtracted. To study the

¹ Based on observations carried out at ESO, La Silla, (Chile) (ESO N. 58, A-0564) and at the Mount Graham International Observatory (AZ) with the VATT: the Alice P. Lennon Telescope and the Thomas J. Bannan Astrophysics Facility.

² Dipartimento di Astronomia, Università di Padova, Vicolo dell'Osservatorio 5, I-35122 Padova, Italy.

³ European Southern Observatory, Alonso de Cordova 3107, Casilla 19001, Santiago 19, Chile.

⁴ Telescopio Nazionale Galileo, Osservatorio Astronomico di Padova, Vicolo dell'Osservatorio 5, I-35122 Padova, Italy.

TABLE 1
PARAMETERS OF THE MODELED GALAXIES

OBJECT NAME (1)	GALAXY TYPE		B_r^0 (mag)	P.A. (deg)	i (deg)	V_{\odot} (km s ⁻¹)	D (Mpc)	SCALE (pc arcsec ⁻¹)	$M_{R,bulge}$ (mag)	M (10 ⁸ M_{\odot})
	RSA (2)	RC3 (3)								
NGC 2179 ^a	Sa	SAS0	12.83	170	51	2885 ± 15	35.6	172.6	-19.07	10
NGC 5064 ^a	Sa	PSA2*	11.67	38	65	2980 ± 15	36.7	177.9	-19.78	<0.5
NGC 4343 ^b	SAT3*	12.37	133	78	1002 ± 10	17.0	82.4	-17.24	5
NGC 4435 ^b	SB0 ₁ (7)	LBS0	11.61	13	90	806 ± 10	17.0	82.4	-18.93	10
NGC 4459 ^b	SO ₃ (3)	LAR+	11.21	110	42	1183 ± 10	17.0	82.4	-19.20	10

NOTE.—Col. (2): Morphological classification from Sandage & Tamman 1981. Col. (3): Morphological classification from de Vaucouleurs et al. 1991 (hereafter RC3). Col. (4): Total B magnitude after correcting for extinction and redshift from RC3. Col. (5): Major-axis position angle from RC3. Col. (6): Inclination from Rubin et al. 1997, except for NGC 2179 and NGC 5064 (Tully 1988). Col. (7): Heliocentric systemic velocity derived as the center of symmetry of the gas rotation curve. For NGC 2179 and NGC 5064 it is taken from our data, and for NGC 4343, NGC 4435, and NGC 4459 it is taken from Rubin et al. 1997. Col. (8): Distance of NGC 2179 and NGC 5064 derived from the heliocentric velocity corrected for the motion of the Sun with respect of the Local Group by $\Delta V = 300 \cos b \sin l$ with $H_0 = 75 \text{ km s}^{-1} \text{ Mpc}^{-1}$. The galaxies of the Rubin's sample are members of the Virgo cluster, and we assumed a distance of 17 Mpc (Freedman et al. 1994). Col. (10): Statistical estimate of the absolute B magnitude of the bulge derived following Simien & de Vaucouleurs 1986. Col. (11): Value of the central mass concentration derived as described in § 3.

^a From our sample.

^b From the sample of Rubin et al. 1997.

$H\alpha$ emission line, we subtracted the underlying stellar continuum, which was determined by averaging a 2.5 Å wide region with high signal-to-noise ratio adjacent to the $H\alpha$ line. A constant stellar continuum provides a good match to the underlying distribution within this narrow wavelength range. For the purpose of this Letter, the subtraction of a continuum with the proper $H\alpha$ absorption is not crucial, since the same bidimensional shape is observed also in the [N II] $\lambda 6583$ line. We did not model this line because it falls at the edge of the sensitivity curve.

In addition to the spectroscopic material, narrowband $H\alpha$ imaging of NGC 2179 was performed on 1997 March 9–11 at the 1.8 m Vatican Advanced Technology Telescope. A back-illuminated 2048 × 2048 Loral CCD with $15 \times 15 \mu\text{m}^2$ pixels was used as detector at the aplanatic Gregorian focus, $f/9$. It yielded a field of view of $6'.4 \times 6'.4$ with an image scale of $0''.4 \text{ pixel}^{-1}$ after a 2×2 on-line pixel binning. We obtained 3×10 minute emission-band images and 3×2 minute Cousins R -band images. The emission-band images were taken with an interference filter ($\lambda_c = 6630 \text{ \AA}$; $\Delta\lambda_{\text{FWHM}} = 70 \text{ \AA}$), isolating the spectral region characterized by the redshifted $H\alpha$ and [N II] $\lambda\lambda 6548, 6583$ emission lines. The data reduction was routine. A Gaussian fit to field stars in the two final processed

images yielded a point-spread function (PSF) FWHM of $1''.0$. The continuum-free image of NGC 2179 showing the galaxy $H\alpha + [\text{N II}]$ emission was obtained by subtracting the R -band image, suitably scaled, from the emission-band image.

3. RESULTS

The complex bidimensional structure (in the velocity-position map) of the $H\alpha$ emission line in NGC 2179 is shown in Figure 1a. In the central region ($r \lesssim 2''$), the line is highly tilted, suggesting fast rotation (at $r = \pm 0''.6$ we measure $\Delta v \approx 200 \text{ km s}^{-1}$), and the wings extend up to $\pm 250 \text{ km s}^{-1}$. The intensity distribution along the line shows two symmetric peaks and a central minimum at $r = 0, v = 0$. The shape of the emission is such that at $r = \pm 3''$, we observe $\Delta v \approx 200 \text{ km s}^{-1}$. Proceeding further away from the center, Δv increases up to an almost constant value of 400 km s^{-1} .

In the following, we demonstrate that the peculiar shape and intensity distribution of these emission lines is not produced by two kinematically distinct components as the appearance could suggest, but they are due to a unique velocity field traced by a thin gaseous disk rotating in the combined potential of a central pointlike mass ($v \rightarrow \infty$ as $r \rightarrow 0$) embedded in an ex-

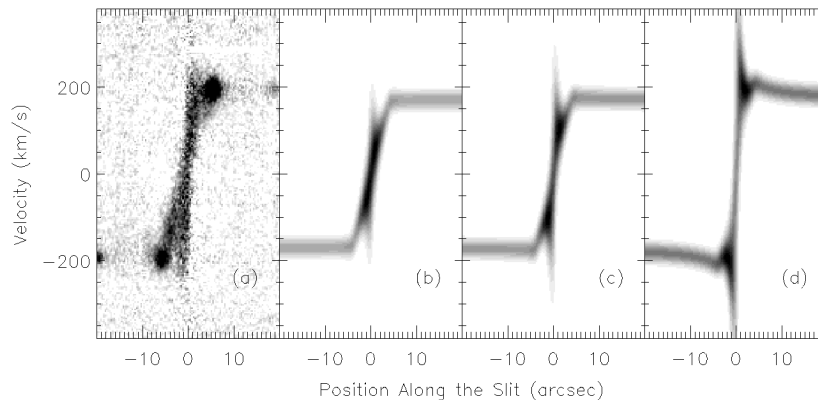


FIG. 1.—(a) $H\alpha$ emission line, observed along the major axis of NGC 2179, after subtraction of the stellar continuum. (b, c, d) Models of the NGC 2179 $H\alpha$ line (shown in the same scale of a) obtained with different pointlike central masses: (b) $M = 2 \times 10^8 M_{\odot}$; (c) $M = 1 \times 10^9 M_{\odot}$, corresponding to our best-fit model; (d) $M = 5 \times 10^9 M_{\odot}$.

tended stellar disk and to the deterioration caused by the instrumental resolution and seeing. The presence of a gaseous disk in the principal plane of NGC 2179 is supported by our H α image, which shows a smooth central structure characterized by the same ellipticity ($\epsilon \approx 0.2$) and major-axis position angle (P.A. $\approx 170^\circ$) as those of the stellar content observed in the R -band. The bright knots present in the observed spectrum are due to spiral arms, which are also visible in our H α image.

We assume that the gas resides in an infinitesimally thin disk whose mean motion is characterized by circular orbits in the plane of the galaxy. At each position (x, y) on the sky, the line-of-sight velocity profile is a Gaussian ϕ with mean $V(x, y) = V_c(R)x \sin i/R$ and dispersion $\sigma(R)$, where $R^2 = x^2 + (y/\cos i)^2$ is the radius in the disk and i (Table 1) is the inclination of the galaxy. The dispersion is given by $\sigma^2(R) = \sigma_{\text{gas}}^2(R) + \sigma_{\text{instr}}^2$, where $\sigma_{\text{gas}}(R)$ is the intrinsic velocity dispersion of the gas and σ_{instr} is the instrumental dispersion (assuming a Gaussian instrumental broadening function). The gas dispersion is assumed to be isotropic and has been parametrized through $\sigma_{\text{gas}}(R) = \sigma_0 + \sigma_1 \exp(-R/R_t)$. The best-fit values of the scale length of the turbulence R_t , and of the parameters σ_0 and σ_1 reproducing the observed data give rise to a dispersion profile that is only moderately peaked. This is confirmed by the fact that the intensity along the line has a minimum in the center ($v = 0, r = 0$) due to the high redshift and blueshift of the radiation close to the central mass concentration.

The circular velocity $V_c(R)$ is produced by the combined potential of a pointlike mass M , and of the disklike stellar component. The contribution to the velocity due to the pointlike mass is given by $V_*(R) = (GM_*/R)^{1/2}$. The contribution $V_*(R)$ due to the stars' potential has been directly measured on the emission lines of each spectrum at distances at which both the seeing effect and the pointlike mass attraction are negligible, and it has been linearly interpolated for smaller R by imposing that $V_*(0) = 0$. The linearity of this interpolation implies that the central core is homogeneous. As a consequence, the stellar mass present in the central region results underestimated, since we know from HST observations that galaxies typically have density that increases toward the center. We have calculated that, even considering an extreme central cusp so far observed, the central pointlike mass results decreased by no more than 10%. The resulting intrinsic velocity profile of the disk is then computed as $V_c^2(R) = V_c^2(R) + V_*^2(R)$.

The bidimensional model of the emission lines is given by

$$\Phi(v, S) = \int_{S-(\Delta s/2)}^{S+(\Delta s/2)} ds \int_{B-(h/2)}^{B+(h/2)} db \int_{-\infty}^{+\infty} \{I(s', b') \times \phi[v - V(s', b')]P(s' - s, b' - b)\} ds' db', \quad (1)$$

where (S, B) are the coordinates along the slit and perpendicular to it, respectively, while h is the slit width and Δs is the pixel size of the detector. $I(s', b')$ is the intrinsic surface brightness distribution of the disk and has been parametrized as $I(R) = I_0 + I_1 \exp(-R/R_t)$, where I_0 , I_1 , and R_t are free parameters. $P(s' - s, b' - b)$ is the PSF, which has been modeled as a Gaussian owing to the lack of a specific PSF image obtained at the time of the observations. Note that the parameterizations for $I(R)$ and $\sigma_{\text{gas}}(R)$ have been chosen because they are able to adequately reproduce our data, but they have no further physical significance.

The line profile $\Phi(v, S)$, rebinned on a grid with steps Δv (reciprocal dispersion) and Δs , can be directly compared to the

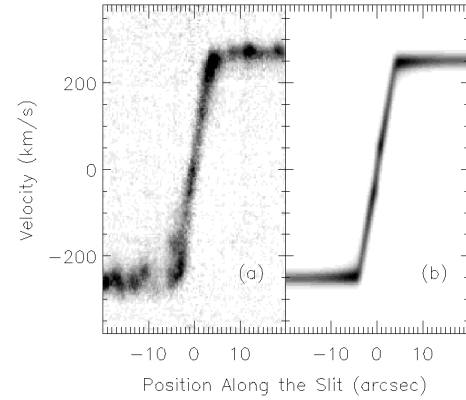


FIG. 2.—(a) H α emission line, observed along the major axis of NGC 5064, after subtraction of the stellar continuum. (b) Model of the NGC 5064 H α line obtained with the highest pointlike central mass that can be added without significantly disturbing the general shape of the line ($M_* = 5 \times 10^7 M_\odot$).

star-light-subtracted bidimensional spectrum obtained on the CCD. Using the above model and the distance given in Table 1, we have obtained for NGC 2179 the simulation of the H α emission line shown in Figure 1c, which is remarkable for its similarity with the observed one (Fig. 1a). The bright knots in the spectrum due to the spiral arms have not been reproduced in our model. The pointlike mass of the best-fit model is $1 \times 10^9 M_\odot$. It should be clear that our model shows only the consistency of the observations with the presence of a central pointlike mass (black hole). However, a central stellar density cusp could also fit the data. In order to estimate the errors in the central mass determination, we have modeled the shape of the line for different central pointlike masses. In Figures 1b and 1d, we show two extreme cases in which the central mass is smaller and larger, respectively, by a factor of 5 than the mass of the best fit. On the basis of visual comparison with the observations of a series of models, we estimate that our error could not be larger than a factor of 3 ($\log M_* = 9.0 \pm 0.5$ in solar units).

The bidimensional shape of the H α emission line in the second galaxy we observed, NGC 5064, is shown in Figure 2a. Contrary to NGC 2179, it does not present any peculiar central structure. The line gives rise to a standard rotation curve with the inner rigid-body rotation extended up to $r = \pm 4''$ and followed by a flat portion ($\Delta v \approx 400 \text{ km s}^{-1}$). By applying the same modeling technique as we did for NGC 2179, we computed the shape of the emission lines as a function of decreasing central mass until the complex structure described above tends to disappear. The limiting case corresponds to a central pointlike mass of $5 \times 10^7 M_\odot$ and is illustrated in Figure 2b. Comparing this model with the observed H α line in NGC 5064, we deduce that in this galaxy either the central mass is lower than $5 \times 10^7 M_\odot$ or the unresolved Keplerian part of the gaseous disk does not give a detectable contribution.

Emission lines with a bidimensional shape and an intensity distribution similar to those observed in NGC 2179 have been observed also by Rubin et al. (1997) and by Sofue et al. (1998). We have selected in the sample of Rubin et al. (1997) the most representative ones, namely NGC 4343 (Sb), NGC 4435 (S0), and NGC 4459 (S0). We applied our modeling techniques to reproduce their isophotal maps, taking into account their instrumental setup and seeing condition. The comparison between the observations and our models is shown in Figure 3, and it

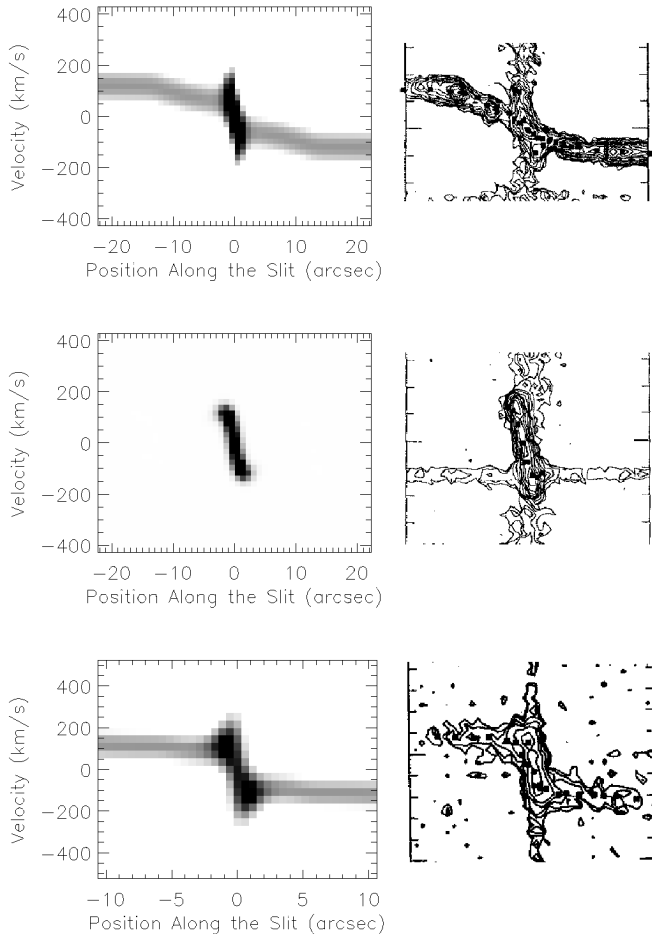


FIG. 3.—Best-fit models (left column) of the $H\alpha$ emission lines observed (their isophotal maps with the same scale are shown in the right column) by Rubin et al. (1997) along the major axis of NGC 4343 (top), NGC 4435 (middle), and NGC 4459 (bottom).

appears quite satisfactory. In all three cases, the central tilted part of the emission is characterized by the absence of a central intensity peak, both in the model and in the observed line. The absence of the flat region of the rotation curve produced by the potential of the stellar disk in the case of NGC 4435 can be easily modeled by adopting $I_0 \approx 0$. The values of the central masses are of the same order as that of NGC 2179 and are given in Table 1. A comparison between a set of model lines

obtained with different central masses and the observations has been carried out for these galaxies, in the same way as we did for NGC 2179. We estimate that the masses given in Table 1 for the Rubin et al. (1997) galaxies are affected by uncertainties of the same order of magnitude as in NGC 2179.

4. DISCUSSION

In the previous paragraphs, we have shown that the peculiar bidimensional shape of the emission lines in a sample of four galaxies is consistent with the effect produced by the combined potential of a central pointlike mass and of an extended component. In this way, we were able to point out the presence of central mass concentrations of the order of $10^9 M_\odot$ in a sample of disk galaxies, observed with ground-based telescopes.

With the observations presented in this Letter, we demonstrate the possibility of detecting central mass concentrations in galaxies with properly equipped ground-based telescopes, using the CNKDs as probes. The masses that can be detected in this way are larger than $5 \times 10^7 M_\odot$ at the distance of the Virgo cluster. Up to now the higher resolution offered by *HST* has not contributed to the detection, using CNKDs, of central masses lower than this limit. In fact, the four galaxies so far studied with *HST* possess central masses of the same order of ours. A simulation similar to the one used in this Letter predicts that *HST*, equipped with the Space Telescope Imaging Spectrograph, will allow detection of central masses down to the level of $5 \times 10^6 M_\odot$. Note that although VLBI spectroscopy of H_2O masers delivers much higher angular resolution, this technique is limited by the availability of suitably bright sources. We are inclined to think that the detection of lower mass black holes will constitute one of the most proper uses of *HST*, which also allows us to put more stringent constraints on the size of the region containing the central mass.

For the four galaxies of this Letter with positive detection, we can summarize our measurements with a single median value of the ratio of the central mass to the luminosity of the bulge component: $M/L_{B, \text{bulge}} \sim 0.16$. This value is 1 order of magnitude larger than the median value derived by Ho (1998) from a sample of 20 objects but is still within the scatter. If we assume for M , of NGC 5064 the upper limit we derived, this galaxy also falls within the scatter of the relation $M-L_{B, \text{bulge}}$ (Ho 1998).

We thank Dave Burstein and Vera Rubin for helpful discussions. J. C. V. B. acknowledges the support by a grant from the Telescopio Nazionale Galileo.

REFERENCES

- Bower, G. A., et al. 1998, *ApJ*, 492, L111
 de Vaucouleurs, G., de Vaucouleurs, A., Corwin, H. G., Jr., Buta, R. J., Paturel, G., & Fouqué, R. 1991, *Third Reference Catalogue of Bright Galaxies* (New York: Springer) (RC3)
 Ferrarese, L., Ford, H. C., & Jaffe, W. 1996, *ApJ*, 470, 444
 Freedman, W. L., et al. 1994, *Nature*, 371, 757
 Greenhill, L. J., & Gwinn, C. 1997, *Ap&SS*, 248, 261
 Greenhill, L. J., Moran, J. M., & Herrnstein, J. R. 1997, *ApJ*, 481, L23
 Ho, L. C. 1998, in *Observational Evidence for Black Holes in the Universe*, ed. S. K. Chakrabati (Dordrecht: Kluwer), in press
 Kormendy, J., & Richstone, D. 1995, *ARA&A*, 33, 581
 Macchetto, F., Marconi, A., Axon, D. J., Capetti, A., Sparks, W., & Crane, P. 1997, *ApJ*, 489, 579
 Miyoshi, M., Moran, J., Herrnstein, J., Greenhill, L. J., Nakai, N., Diamond, P., & Inoue, M. 1995, *Nature* 373, 127
 Rubin, V. C., Kenney, J. D. P., & Young, J. S. 1997, *AJ*, 113, 1250
 Sandage, A., & Tammann, G. A. 1981, *A Revised Shapley-Ames Catalog of Bright Galaxies* (Washington: Carnegie Institution)
 Simien, F., & de Vaucouleurs, G. 1986, *ApJ*, 302, 564
 Sofue, Y., Tomita, A., Tutui, Y., Honma, M., Takeda, Y. 1998, *PASJ*, in press (astro-ph/9807340)
 Tully, R. B. 1988, *Nearby Galaxies Catalog* (Cambridge: Cambridge Univ. Press)
 van der Marel, R. P., & van den Bosch, F. C. 1998, *AJ*, submitted (astro-ph/9804194)